Electronic Supplementary Material (ESI) for New Journal of Chemistry.

Pyran Based Bipodal D-π-A Systems: Colorimetric and Ratiometric Sensing of Mercury; Experimental and Theoretical Approach

Pookalavan Karicherry Vineetha[a], Aravind Krishnan[b], Ajayakumar Aswathy[a], Parvathy O Chandrasekaran[a], Narayanapillai Manoj[a]*

Supporting Information

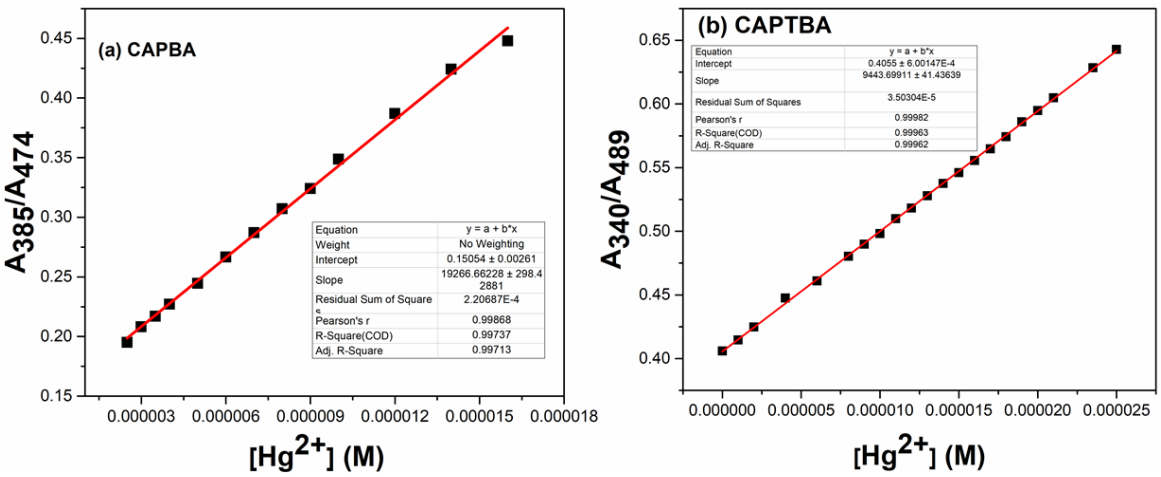

Figure S1 Ratiometric plot of absorbance changes at 385 nm and 474 nm for CAPBA and determination lowest limit of detection by linear fit analysis. a) A plot of absorbance ratio (A_{385}/A_{474}) of CAPBA *vs* concentrations of Hg^{2+} ions in MeCN and (b) A plot of absorbance ratio (A_{340}/A_{489}) of CAPTBA *vs* concentrations of Hg^{2+} ions in MeCN.

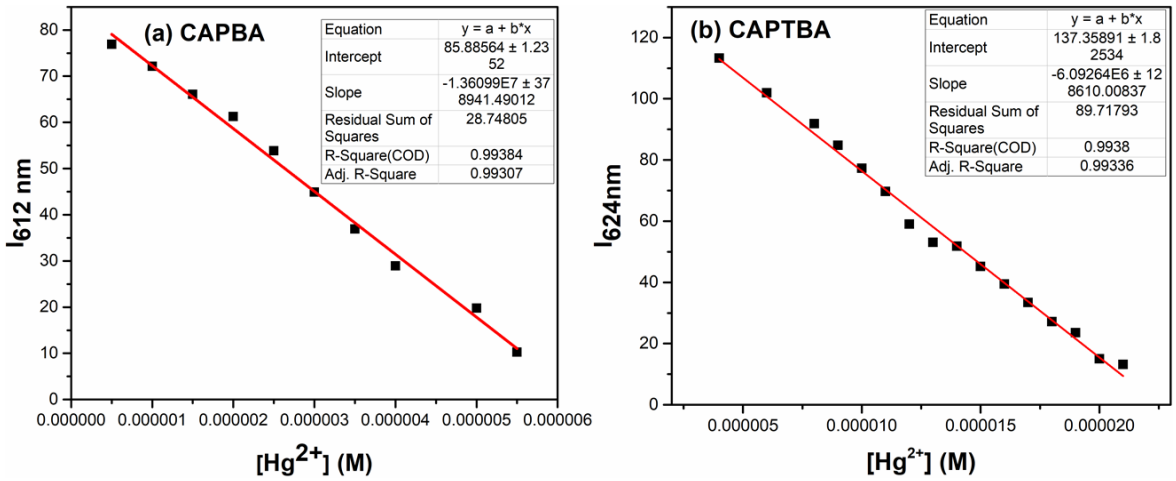

Figure S2: Determination of lowest limit of detection by linear fit analysis. (a) A plot of the emission intensity at 612 nm of CAPBA *vs* concentration of the Hg^{2+} ions (b) A plot the emission intensity at 624 nm *vs* concentrations of Hg^{2+} in MeCN.

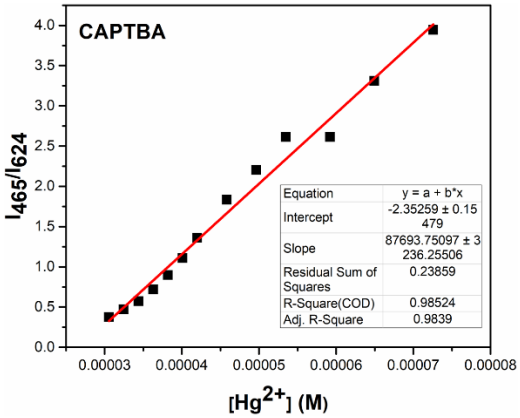

Figure S3: Ratiometric plot of fluorescence changes at 465 nm and 624 nm (I_{465}/I_{624}) of CAPTBA *vs* concentrations of Hg^{2+} ions in MeCN (λ_{ex} = 419 nm) and determination lowest limit of detection by linear fit analysis.

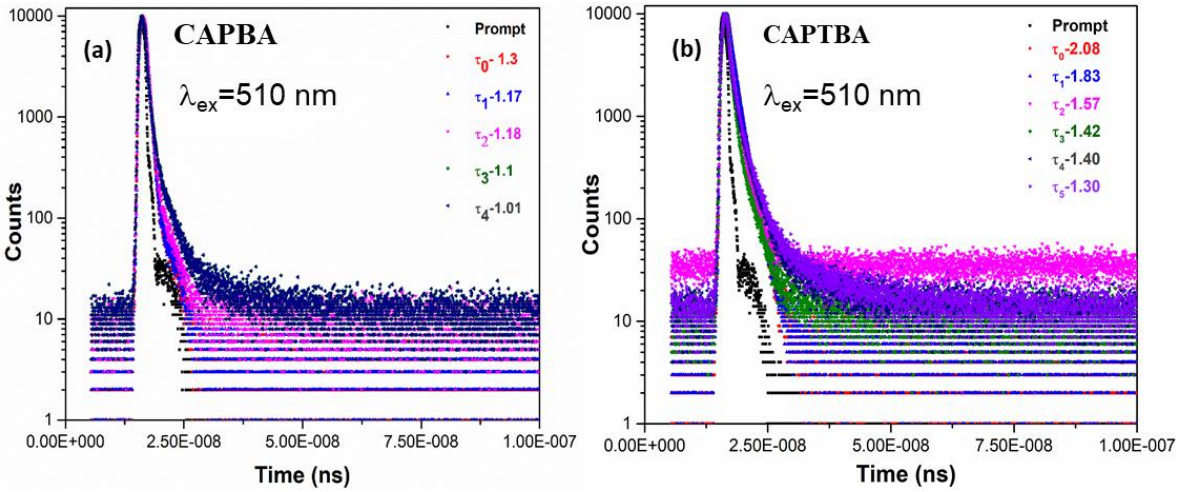

Figure S4: Fluorescence decay-profiles of (a) CAPBA and CAPBA - Hg^{2+} ion complex (λ_{em}=602 nm) (b) CAPTBA and CAPTBA - Hg^{2+} ion complex (λ_{em}= 643 nm); λ_{ex} = 510 nm.

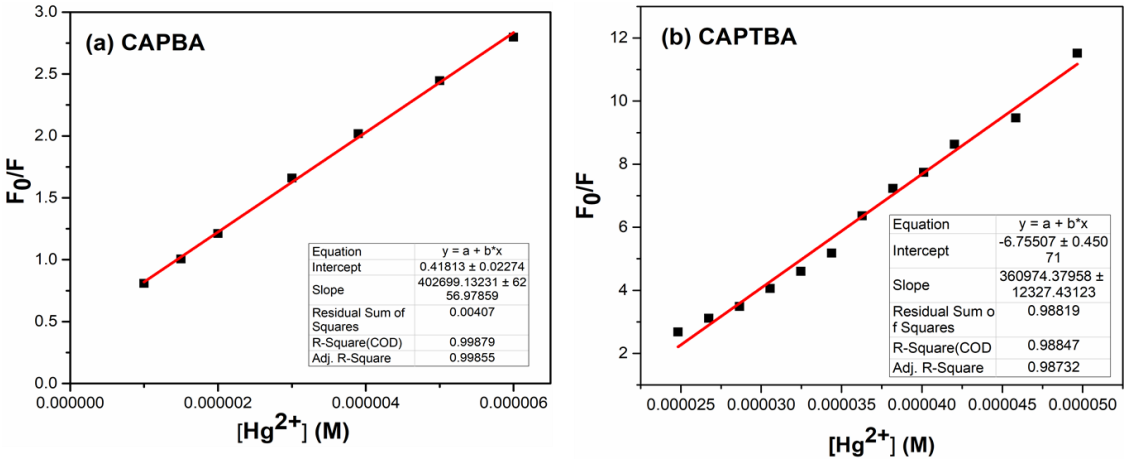

Figure S5: Stern-Volmer plot for fluorescence quenching obtained for (a) CAPBA (7.8 μM) and (b) CAPTBA (6.2 μM) in the presence of increasing concentration of an aqueous solution of Hg^{2+} ions in MeCN (0–15.0 μM) solution

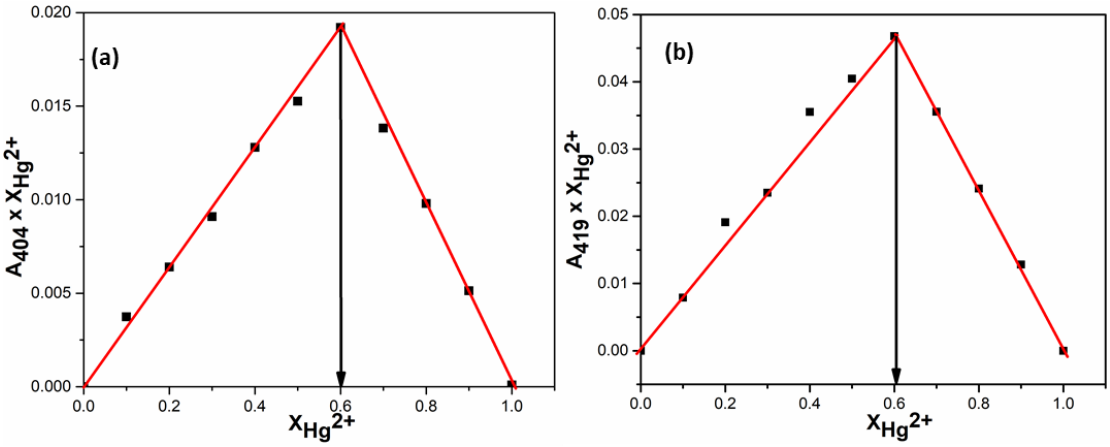

Figure S6: Job plot analysis of CAPBA and CAPTBA with Hg^{2+} ions showing a 1:2 binding stoichiometry in MeCN solution.

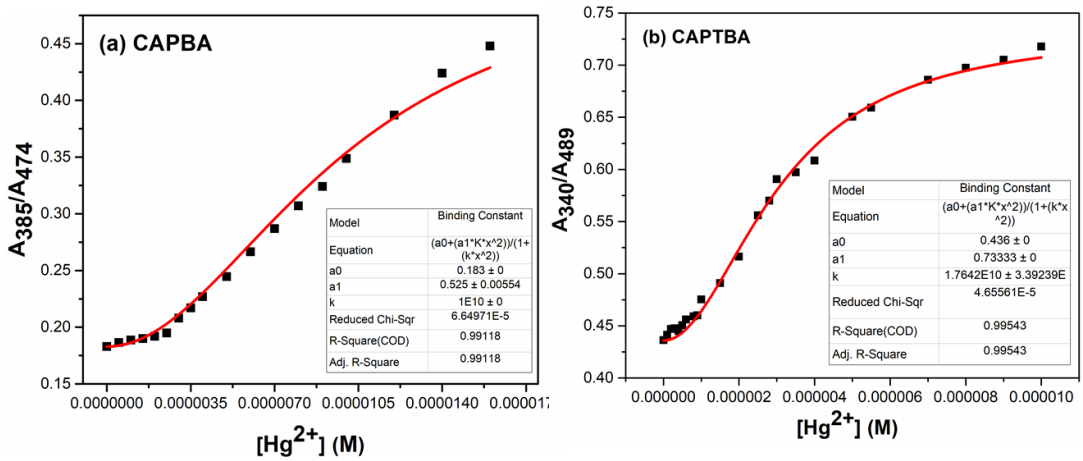

Figure S7: Determination of association constant by nonlinear least square fit analysis. A plot of (a) absorbance ratio of CAPBA (A_{385}/A_{474}) *vs* concentrations of Hg^{2+} ions in MeCN and (b) absorbance ratio of CAPTBA (A_{340}/A_{489}) *vs* concentrations of Hg^{2+} ions in MeCN.

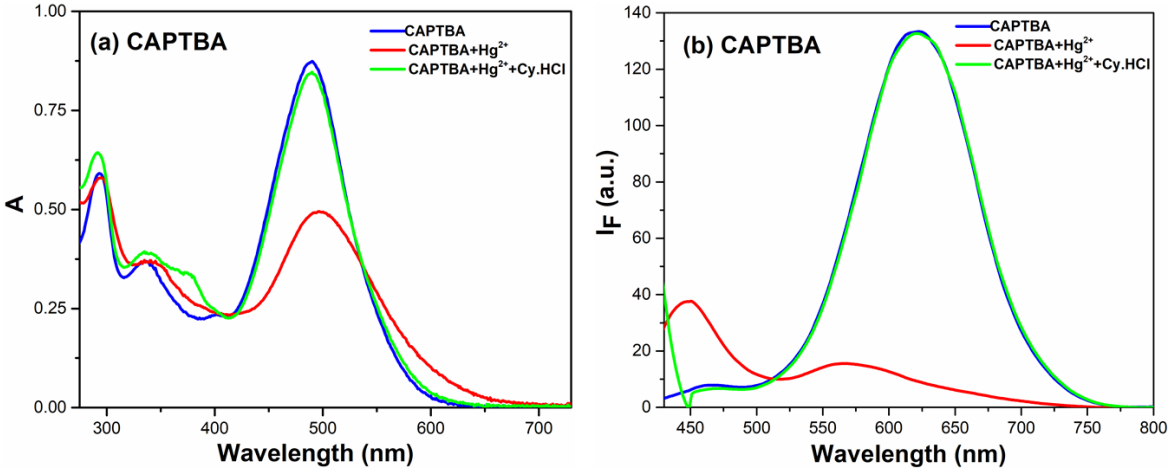

Figure S8: Reversibility of complexation: (a) Absorption spectra of CAPTBA, CAPTBA–Hg^{2+} ion complex and (b) emission spectra of CAPTBA–Hg^{2+} ion complex in the presence of cysteamine hydrochloride in MeCN; λ_{ex} = 419 nm.

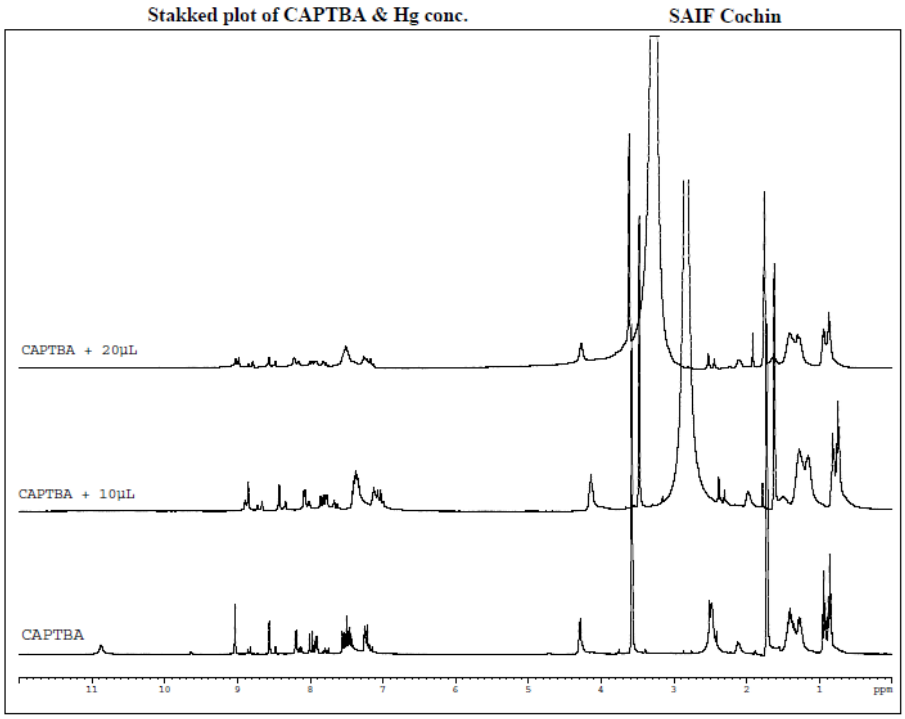

Figure S9: ^{1}H-NMR spectra of CAPTBA and CAPTBA in the presence of 0–2 equivalents of Hg^{2+} acetate (400 MHz, THF-d_8).

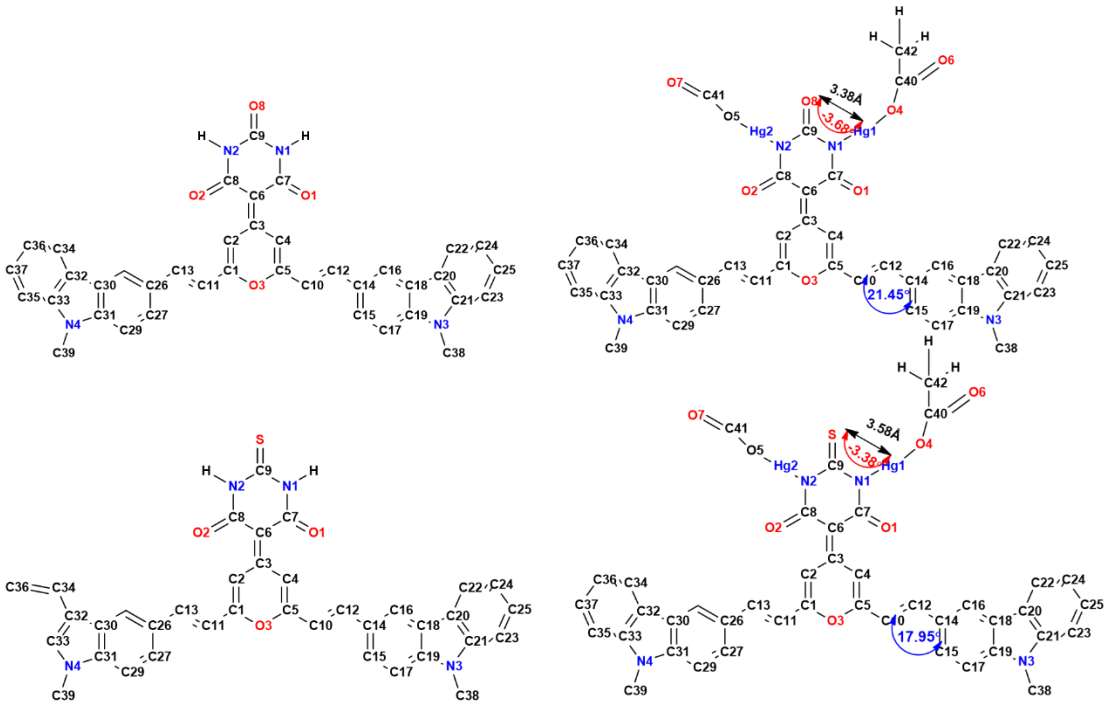

Figure S10. Selected geometrical parameters of the DFT optimized structures of the complexes in MeCN.

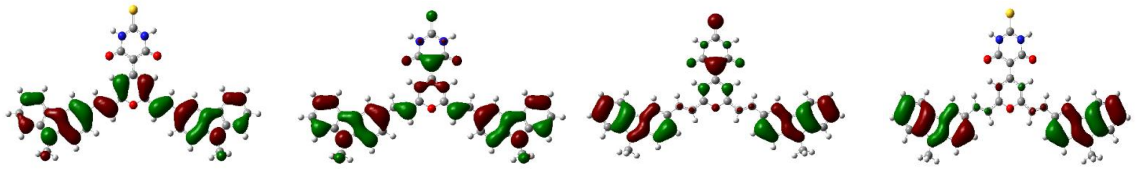

HOMO **-6.79 eV**

HOMO-1 **-7.00 eV**

HOMO-2 **-7.53 eV**

HOMO-3 **-7.54 eV**

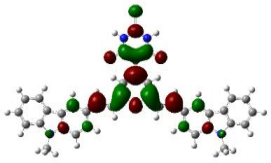

LUMO **-71.79 eV**

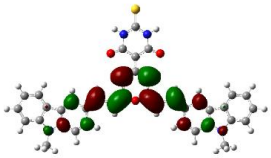

LUMO+1 **-1.00 eV**

Figure S11. Frontier molecular orbitals of CAPTBA (CAMB3LYP).

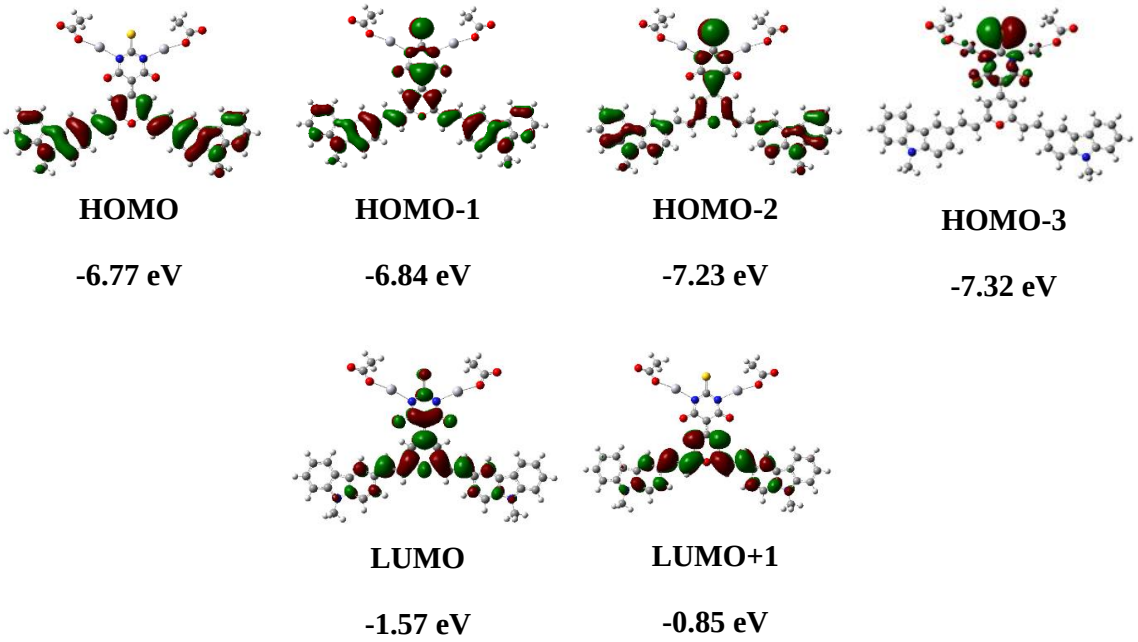

Figure S12. Frontier molecular orbitals of CAPTBA-Hg^{2+} ion complex (CAMB3LYP).

Table S1 Lowest limit of detection obtained by various methods

Probe	Ratiometry (UV)	Colorimerty	Fluorimetry
CAPBA	4.2 μM (±0.04)	3.3 μM (±0.08)	4.76 nM (±0.02)
CAPTBA	2.6 μM (±0.03)	1.2 μM (±0.04)	1.80 nM (±0.06)

Table S2 Fragment ions observed in MALDI-TOF mass spectrum of CAPBA.

(1)	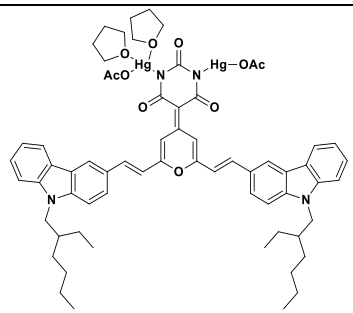	1474.497
(2)	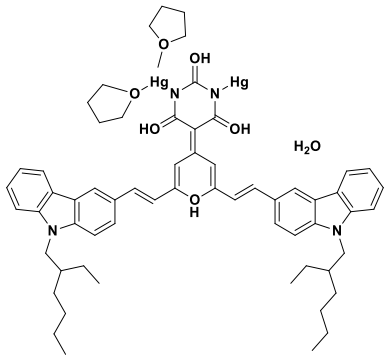	1380.333
(3)	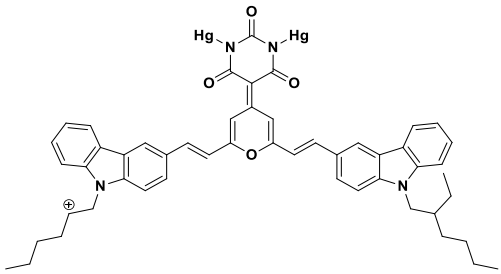	1185.316
(4)	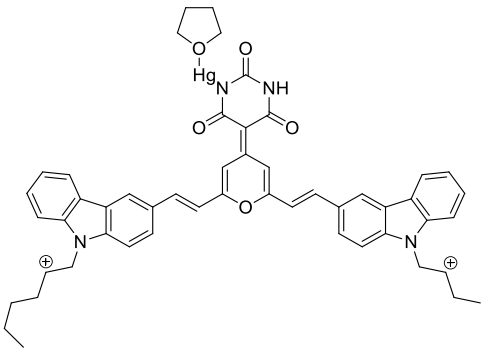	999.340
(5)	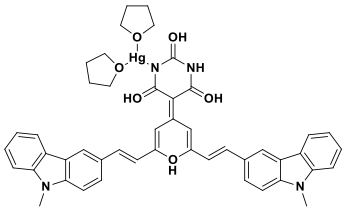	965.320

Table S3. Comparison of experimental and theoretical absorption spectra

Dye	λ_{abs}, (nm) (ε_{max} x 10^4) MeCN	λ_{abs}, (nm), B3LYP (*f*) MeCN	Transitions	λ_{abs}, (nm), CAMB3LYP (*f*) MeCN	Transitions
CAPBA	474 (5.82±0.1)	546 (0.91)	HOMO → LUMO	553 (1.91)	HOMO → LUMO
	335(2.64±0.1)	486 (0.56)	HOMO-1 → LUMO	390 (1.07)	HOMO-1 → LUMO
		382 (0.72)	HOMO → LUMO+1	345 (0.01)	HOMO → LUMO+1
CAPBA-Hg^{2+} complex	474	560 (1.84)	HOMO → LUMO	531 (2.23)	HOMO → LUMO
	340	522 (0.88)	HOMO-1 → LUMO	442 (1.04)	HOMO-1 → LUMO
		444 (0.15)	HOMO → LUMO+1	357 (0.04)	HOMO → LUMO+1
CAPTBA	489 (7.72±0.1)	571 (0.89)	HOMO → LUMO	520 (2.26)	HOMO → LUMO
	340 (3.10±0.1)	507 (0.67)	HOMO-1 → LUMO	437 (1.07)	HOMO-1 → LUMO
		427 (0.24)	HOMO → LUMO+1	352 (0.03)	HOMO → LUMO+1
CAPTBA-Hg^{2+} complex	498	579 (1.87)	HOMO → LUMO	522 (1.98)	HOMO → LUMO
	340	542 (0.95)	HOMO-1 → LUMO	420 (1.39)	HOMO-1 → LUMO
		482 (0.03)	HOMO → LUMO+1	351 (0.03)	HOMO → LUMO+1